

Crustal anisotropy in the Bohemian Massif, Czech Republic: Observations based on Central European Lithospheric Experiment Based on Refraction (CELEBRATION) 2000

Bohuslav Růžek, Václav Vavryčuk, Pavla Hrubcová, Jan Zedník, and the CELEBRATION Working Group¹

Geophysical Institute, Academy of Sciences of the Czech Republic, Prague, Czech Republic

Received 14 October 2002; revised 14 March 2003; accepted 4 April 2003; published 23 August 2003.

[1] We study the azimuthal velocity variation of Pg waves in the Bohemian Massif using data collected during Central European Lithospheric Experiment Based on Refraction (CELEBRATION) 2000. We analyze travel times of waves generated by 28 shots and recorded by 256 portable and 19 permanent seismic stations deployed on the territory of the Czech Republic and in adjacent areas. We use recording offset ranging from 30 to 190 km with azimuths covering the whole interval of angles. The observed travel times are inverted for parameters of a velocity model formed by an isotropic low-velocity subsurface layer with a varying depth lying on a homogeneous transversely isotropic half-space with a horizontal axis of symmetry. The recovered velocity displays a systematic azimuthal variation indicating a regional-scale intrinsic or effective anisotropy in the Bohemian Massif. The mean, minimum and maximum values of the velocity are $v_{\text{mean}} = 6.03$ km/s, $v_{\text{min}} = 5.98$ km/s, $v_{\text{max}} = 6.10$ km/s, respectively, indicating an anisotropy of 1.5–2.5%. The direction of the maximum propagation velocity is $\sim N35^\circ E$ being approximately perpendicular to the present maximum compression in the Earth crust in central Europe. The observed anisotropy cannot be induced by stress-aligned cracks in the crust, because the crack models predict azimuthal velocity variations completely inconsistent with the observed one. Therefore we suggest the crustal anisotropy to be induced by a preferred orientation of rock-forming minerals and large-scale intrusion fabrics developed during a tectonic evolution of the Bohemian Massif. *INDEX TERMS*: 0905 Exploration Geophysics: Continental structures (8109, 8110); 0935 Exploration Geophysics: Seismic methods (3025); 7205 Seismology: Continental crust (1242); 7218 Seismology: Lithosphere and upper mantle; *KEYWORDS*: anisotropy, Earth crust, seismic waves, refraction

Citation: Růžek, B., V. Vavryčuk, P. Hrubcová, J. Zedník, and the CELEBRATION Working Group, Crustal anisotropy in the Bohemian Massif, Czech Republic: Observations based on Central European Lithospheric Experiment Based on Refraction (CELEBRATION) 2000, *J. Geophys. Res.*, 108(B8), 2392, doi:10.1029/2002JB002242, 2003.

1. Introduction

[2] Many observations indicate seismic anisotropy as a ubiquitous property of the Earth crust and upper mantle, which is detected on local as well as regional scales using various types of seismic waves [Babuška and Cara, 1991; Savage, 1999; Weiss *et al.*, 1999]. The anisotropy of the Earth crust is mostly caused by sediment layering, by stress-aligned systems of microcracks, cracks or fractures, by deformation and faulting of the crust, or by textural ordering of rock-forming minerals in the crust. Crustal anisotropy is studied in the laboratory by measuring P and S wave velocities on rock samples, or in situ using

arrivals of P and S waves, splitting of S waves or using surface waves.

[3] So far, crustal anisotropy in the Bohemian Massif and adjacent areas has been measured mainly locally at various isolated sites. It has been measured mostly under laboratory conditions on rock samples from West Bohemia [Pros *et al.*, 1998; Martínková *et al.*, 2000; Chlupáčová *et al.*, 2003] and from the KTB drill hole [Kern and Schmidt, 1990; Kern *et al.*, 1991; Jahns *et al.*, 1996; Berckhemer *et al.*, 1997]. These measurements show a rather high scatter of P wave anisotropy and orientation of its axes in dependence on the site and type of rock measured. Also, results for shear wave anisotropy obtained from in situ experiments based on shear wave splitting analysis in West Bohemia [Vavryčuk, 1993, 1995] and at the KTB site [Rabbel, 1994; Rabbel and Mooney, 1996] indicate that the strength of anisotropy can vary significantly within the area under study. Nevertheless, the orientation of anisotropy axes from in situ experiments

¹A. Guterch, M. Grad, G. R. Keller, K. Posgay, J. Vozár, A. Špičák, E. Brueckl, Z. Hajnal, H. Thybo, and O. Selvi.

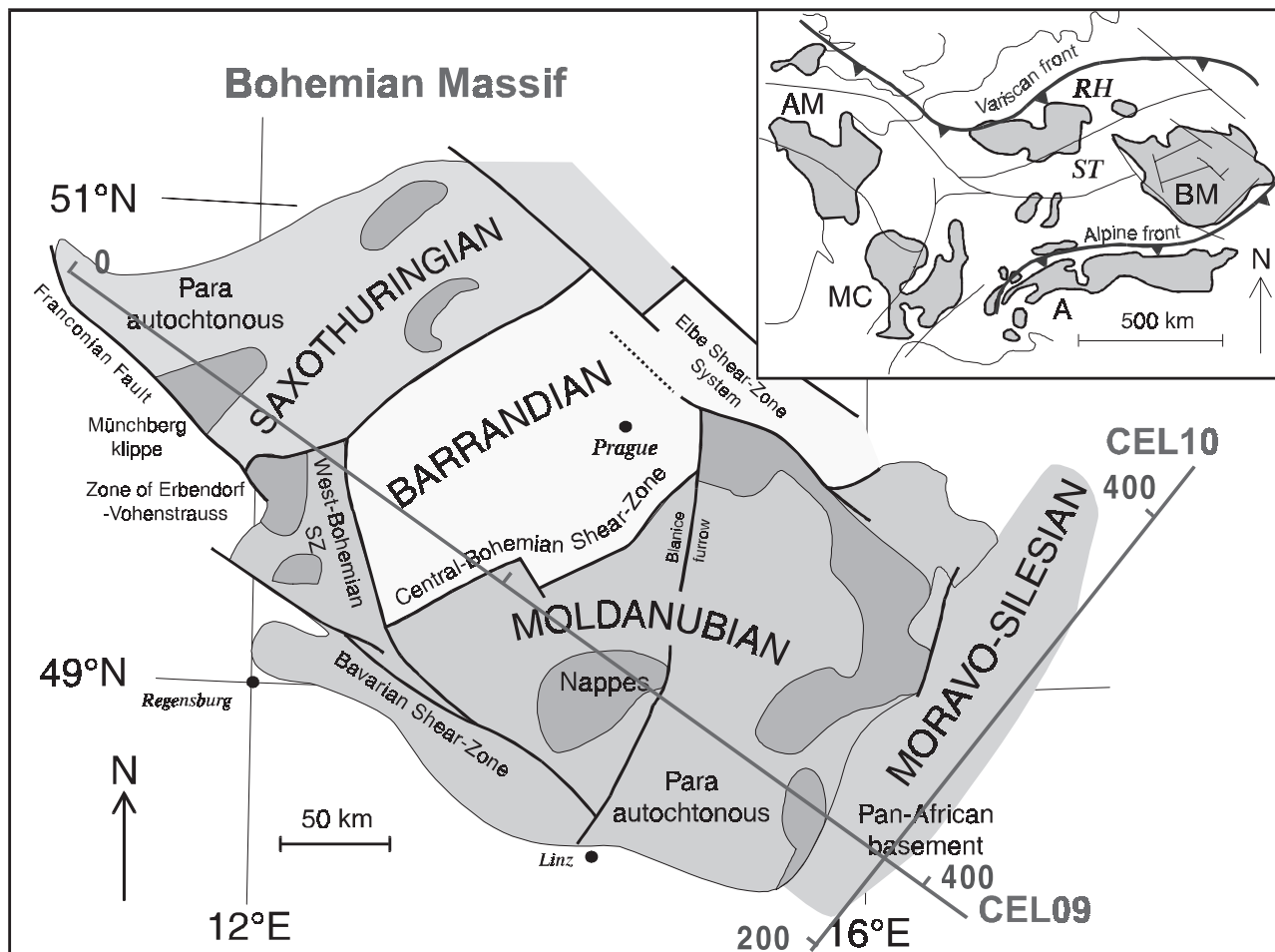


Figure 1. Major tectonic units of the Bohemian Massif and its setting within the European Variscides. BM, Bohemian Massif; AM, Armorican Massif; MC, Massif Central; A, Alps; ST, Saxothuringian Zone; RH, Rhenohercynian Zone [after Pitra *et al.*, 1999; Franke *et al.*, 2000].

seems to be more consistent being related to the direction of the maximum horizontal compressive stress in the region. A similar observation has also been made by Plomerová *et al.* [1981, 1984], who studied the regional-scale velocity variation of waves propagating in the Bohemian Massif. They reported some indications of an increase of Pg wave velocities in the NE–SW direction, which is roughly perpendicular to the direction of the maximum compression in the region.

[4] In this paper, we study the upper crustal azimuthal anisotropy of the Bohemian Massif from refraction travel time data collected during Central European Lithospheric Experiment Based on Refraction (CELEBRATION) 2000. We use travel times of Pg waves generated by explosions recorded at distances ranging from 30 to 190 km. The travel times of Pg waves were measured on records of permanent seismic stations, located on the territory of the Czech Republic and in adjacent areas, and of portable seismic stations, deployed during the CELEBRATION 2000 experiment [Guterch *et al.*, 2001; Málek *et al.*, 2001]. Data from the permanent and portable stations were processed separately and the results were compared. The aim of this study is to decide whether the upper crustal azimuthal anisotropy

can be detected on a regional scale, and if so, to estimate its strength and orientation.

2. Geological and Tectonic Settings

[5] The Bohemian Massif is one of largest stable outcrops of pre-Permian rocks in central and western Europe. It forms the easternmost part of the Variscan Belt, which developed approximately between 500 and 250 Ma during a stage of large-scale crustal convergence, collision of continental plates and microplates and possibly also subduction [Matte *et al.*, 1990]. It consists mainly of high-grade metamorphic and plutonic Paleozoic rocks. On the basis of the respective effects of the Cadomian (Pan-African) and Variscan orogenesis, the Bohemian Massif can be subdivided into various zones, Saxothuringian, Barrandian, Moldanubian, and Moravo-Silesian (see Figure 1). Geographically, it comprises the area of the Czech Republic, partly Austria, Germany, and Poland.

[6] The Moldanubian region represents a major crystal-line segment within the Bohemian Massif and its boundary with the Saxothuringian in the NW is regarded to be a major suture-type discontinuity. A structurally higher unit, the

Barrandian, has been thrust over the Saxothuringian rocks toward the northwest, while in the SE it has been thrust in southerly directions over the Moldanubian from which it is separated by a major NE–SW trending Variscan dextral fault, the Central Bohemian Shear Zone [Dallmeyer *et al.*, 1994]. The mostly NE–SW striking Moldanubian/Moravo-Silesian boundary in the east has the character of a major ductile shear zone with a predominance of strike-slip movements. The easternmost part of the Bohemian Massif, the Moravo-Silesian, submerges beneath the Carpathian Foredeep, where it reappears as a basement reactivated during the Alpine orogeny.

[7] From a tectonic point of view, one of the major forming effects was during Variscan orogeny when the Bohemian Massif, as part of Armorica plate, was sandwiched between high-grade Variscan metamorphic areas and initially between two oceanic, then continental, opposing subduction zones [Matte, 2001]. The boundaries between the Saxothuringian and Barrandian and between the Barrandian and Moldanubian crustal domains to the west, as well as, between the Moldanubian and Brunovistulian platform to the east were of NE–SW trending and indicated the direction of corresponding metamorphic and intrusion activities. The oldest (370–380 Ma) deformational fabrics occur in the Barrandian complex; they trend NE–SW and dip to the SE. The development of these structures is associated with earliest stages of the Saxothuringian eastward subduction and shortening of the plate. The upper plate progressively evolved into a lithospheric scale arc system, which culminated at around 350–345 Ma and was manifested by intrusion of the Central Bohemian Plutonic Complex. The intrusion fabrics of this intrusive complex are steeply dipping into the east and parallel to the western boundary of the Barrandian domain. The crustal root of the Moldanubian shows nearly vertical NE–SW trending fabrics (estimated age of 370–330 Ma) developed mostly in granulites and associated mantle slivers [Schulmann *et al.*, 2002].

[8] The Moldanubian segment contains mainly high-grade gneisses and migmatites of supracrustal origin, orthogneisses, granulites and numerous Variscan posttectonic granitoid intrusions. The Barrandian is composed largely of Precambrian sedimentary and volcano-sedimentary sequences overlain unconformably by Early Paleozoic strata. The easternmost part of the Saxothuringian zone belonging to the Bohemian Massif is dominated by relatively low-grade sedimentary and volcanic rocks controlled by a number of large NE trending synforms and antiforms from a late stage of deformation. The Moravo-Silesian includes autochthonous Cadomian basement, Brunovistulicum, with its Devonian to Carboniferous sedimentary cover.

3. Data

[9] A large-scale seismic refraction experiment CELEBRATION 2000 (C2000) was realized on the territory of Poland, the Czech Republic, the Slovak Republic, Austria, Hungary, Germany, Russia, and Byelorussia in June 2000 with the aim of investigating the deep lithospheric structure of central Europe. During the C2000 experiment 147 shots were fired, 1200 portable seismic

stations were distributed along 5400 km of profiles, and about 160 000 seismic records were gathered. The average distance between shots was 30 km with a station spacing of 2.7 km. The positions of shots and stations were checked by GPS; the origin time was controlled by a DCF77 timer with an accuracy of 3 ms. The sensors of portable stations were 4.5 Hz geophones, recording instruments were TEXAN, REFTEK and PDAS provided by the IRIS Consortium under the PASSCAL program, by the University of Texas at El Paso, USA, and by GeoForschungsZentrum Potsdam, Germany.

[10] As part of the C2000 experiment, the region of the Bohemian Massif was studied along two international profiles: C09 and C10. Profile C09 traverses the whole Bohemian Massif in the NW–SE direction: it starts in the NW in the Saxothuringian, transects mafic amphibolite complex intrusion and continues to the Barrandian. Then it crosses the granitoid intrusions spreading along the Central Bohemian Shear Zone and continues to the Moldanubian, Moravo-Silesian and further SE to the Neogene basins and Carpathian Foredeep. Profile C10 is spreading along the eastern edge of the Bohemian Massif in Moravo-Silesian unit being almost perpendicular to C09. Starting in SW it crosses the Brunovistulic crystalline complex and continues to the NE to Carboniferous Paleozoic cover. The purpose of these profiles was to investigate the structure of the Bohemian Massif (C09) and of the transition zone between the Bohemian Massif and the Carpathians (C10).

[11] A total of 40 shots were fired along the C09 and C10 profiles with charges ranging from 210 kg to 10713 kg of explosives. For our purpose, we have analyzed recordings from 14 shots fired along the C09 profile, from 9 shots fired along the C10 profile, and additionally from 5 shots fired off any profile (see Table 1). Hence the geometry comprises 23 inline and 5 offline shots. All shots used in the computations were recorded by two types of instrumentation: by portable and permanent seismic stations (see Figure 2). As the extent and quality of the respective data sets is different, they were processed separately and the results were compared.

3.1. Data From Permanent Stations

[12] Figure 3 shows the ray path coverage for Pg waves observed at permanent stations operated on the territory of the Czech Republic and in adjacent areas. We have used recording offset ranging from 30 to 190 km. A minimum distance of 30 km was applied to eliminate local-scale effects. The upper limit of 190 km represents the maximum distance at which the arrivals of Pg waves, excited by the C2000 explosions, were identified and measured on recordings reliably. The total number of rays is 135. The azimuthal distribution of rays is uniform. Most permanent seismic stations are equipped with three-component broadband sensors and recordings are performed with a sampling frequency of 20 Hz. The corner frequency of the analogue antialias Bessel filter was 5 Hz. The accuracy of picking of arrival times is around 200 ms. This value was assured by exploring the differences between travel times corresponding to doubled explosions (shots fired twice at the same site, see Table 1). The travel times provided by the permanent stations form a nearly

Table 1. List of Shots

Day	Time, UT	Shot ID	Charge, kg	H, m	φ , °N	λ , °E	Territory
<i>Profile C10 Shots</i>							
16	2215:00.000	20092	210	662	49.8716	17.3891	Czech Republic
23	2100:12.320	20070	210	320	49.1449	16.4381	Czech Republic
23	2245:00.000	20100	210	428	50.0757	17.6246	Czech Republic
23	2315:00.000	20080	210	619	49.4464	16.8323	Czech Republic
24	0015:00.000	20081	210	619	49.4464	16.8327	Czech Republic
24	0100:00.000	20090	210	660	49.8721	17.3894	Czech Republic
24	0115:00.000	20091	210	661	49.8719	17.3892	Czech Republic
25	0300:00.223	20060	210	350	48.6033	15.8447	Austria
25	0344:59.730	20050	210	420	48.3404	15.5951	Austria
<i>Profile C09 Shots</i>							
23	1914:30.133	29020	210	526	50.5444	11.7666	Germany
23	1931:12.417	29010	210	270	50.6875	11.5573	Germany
24	2100:00.000	29100	210	476	49.3124	14.5900	Czech Republic
24	2200:00.000	29090	210	474	49.5182	14.1295	Czech Republic
24	2245:00.000	29120	210	612	49.0191	15.3173	Czech Republic
24	2315:00.000	29121	210	615	49.0191	15.3168	Czech Republic
25	0015:00.000	29110	210	492	49.1892	14.9104	Czech Republic
25	0045:00.000	29111	210	492	49.1896	14.9105	Czech Republic
26	0015:00.000	29051	210	679	50.0210	12.9091	Czech Republic
26	0100:00.000	29060	210	661	49.9251	13.0923	Czech Republic
26	0115:00.000	29061	210	661	49.9249	13.0925	Czech Republic
26	0214:59.997	29130	210	459	48.8526	15.6997	Austria
26	0230:00.396	29140	210	417	48.6723	16.1564	Austria
26	0348:05.896	29070	435	545	49.8725	13.1993	Czech Republic
<i>Off-Profile Shots</i>							
23	1900:30.767	29040	413	630	50.1212	12.2250	Czech Republic
24	0315:00.735	26900	160	220	50.5629	13.7243	Czech Republic
25	0315:00.113	26910	200	399	50.2166	12.6683	Czech Republic
25	0329:59.895	26911	3954	399	50.2172	12.6677	Czech Republic
26	0315:00.805	29080	910	446	49.6453	14.3491	Czech Republic

linear time-distance curve (see Figure 3). The mean value of the P_g velocity obtained by the least squares is 6.075 km/s with a standard deviation of arrival times of 422 ms. The offset at zero distance caused by the low-velocity layer is 496 ms.

3.2. Data From Portable Stations

[13] Figure 4 shows the ray path coverage for P_g waves observed at the C2000 portable stations used in our study. The length of the ray paths covers a range of 30 to 150 km. The azimuthal distribution of rays indicates that the distribution is not uniform, because many rays follow the directions of profiles. However, shots fired off the profiles and cross-profile measurements allowed to spread the spatial distribution of rays over the whole range of azimuths. The total number of rays is 1475. The sampling frequency of one-component (vertical) recordings was 100 Hz. The corner frequency of the antialias FIR filter was 40 Hz. The accuracy of the measured arrival times of P_g waves was thus around 50 ms, which shows remarkably higher accuracy than for permanent stations. The travel times form a nearly linear time-distance curve. This indicates that the velocity distribution of the Bohemian Massif has no strong vertical velocity gradient. The mean value of the P_g velocity obtained by the least squares, the standard deviation of arrival times, and the time offset at zero distance attributed to a low-velocity layer are summarized in Table 2. The values are calculated for the whole data set and for the C09 and C10 profiles separately. The table shows that the mean velocity for the C10 profile is slightly

higher than for the C09 profile. This is an indication of a weak anisotropy or slight lateral inhomogeneity present in the Bohemian Massif.

4. Time-Term Method

[14] We assume a homogeneous anisotropic crust covered by a thin low-velocity isotropic layer with a variable thickness and velocity. The total travel time τ_{ij} between shot i and station j is expressed as follows [Bamford, 1977; Song *et al.*, 2001]:

$$\tau_{ij} = a_i + b_j + D_{ij}S, \quad (1)$$

where a_i is the i th shot delay term (“the shot correction”), b_j is the j th station delay term (“the station correction”), D_{ij} is the epicentral distance between shot i and station j , and S is the slowness. The delay terms a_i and b_j represent the time spent by the refracted wave in the low-velocity layer, thus they combine the effect of the thickness of the layer with its

Table 2. Linear Regression of Travel Times

Data Set	Mean Velocity, km/s	Standard Deviation of Time Residuals, ms	Time Offset at Zero Distance, ms
C09 profile	5.964	176	171
C10 profile	6.096	194	446
C09+C10 profiles	6.013	201	279

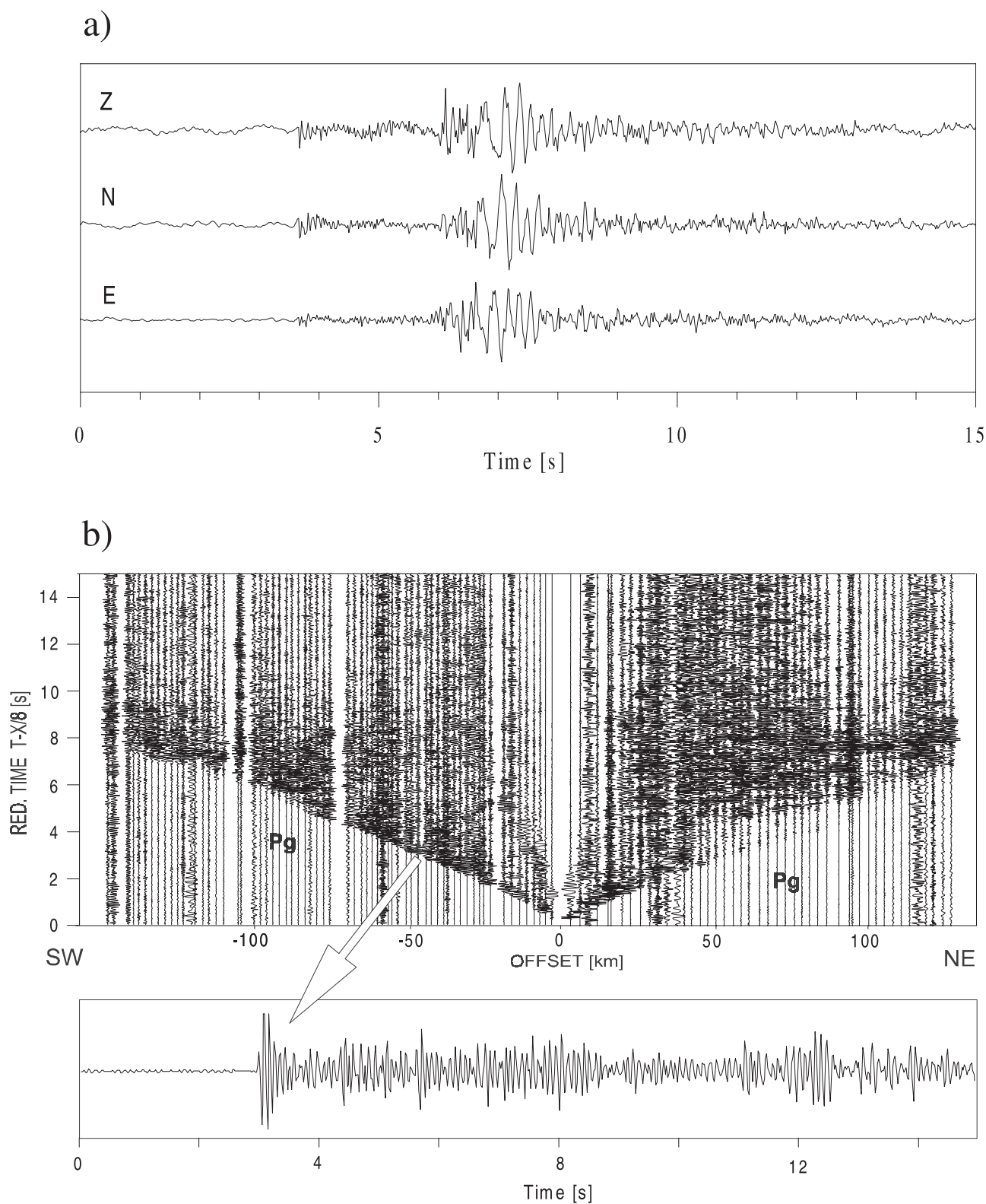


Figure 2. (a) A three-component velocigram recorded at permanent station PRU (shot 29080, epicentral distance 41 km). (b) Vertical velocigrams recorded at portable stations deployed along profile C10 (shot 20080, time is reduced using $v = 8$ km/s).

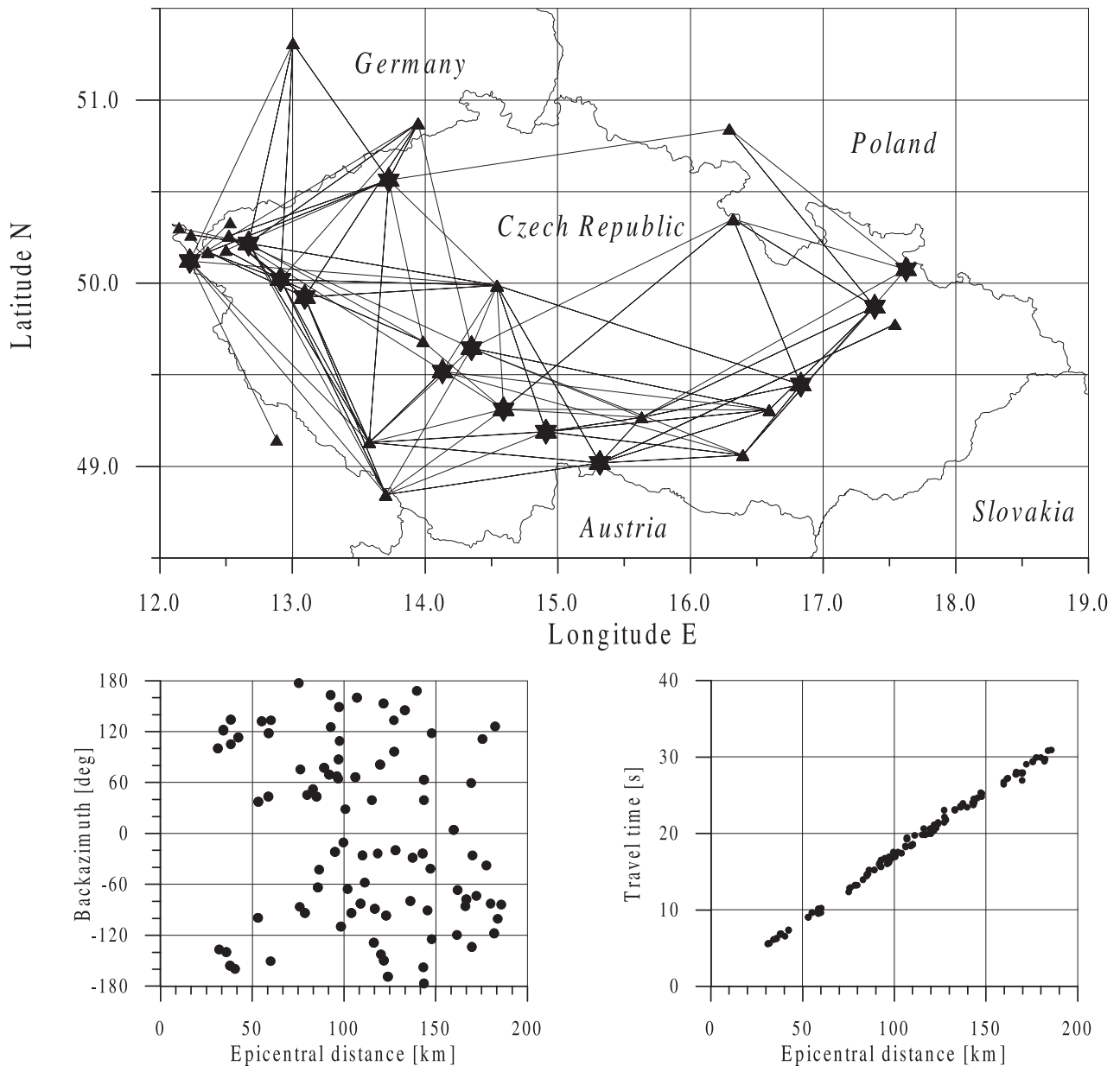


Figure 3. (top) Ray path coverage for waves recorded by permanent seismic stations deployed on the territory of the Czech Republic and in adjacent areas. Shots are marked by stars, and stations by triangles. (bottom left) Azimuth-distance distribution of the data. (bottom right) P_g travel times as a function of epicentral distance (the mean velocity is 6.075 km/s, the offset at zero distance is 496 ms).

velocity beneath each shot and station. The properties of the surface layer can probably vary significantly in the area studied and are considered to be unknown. The delay times may also reflect systematic errors in timing or phase identification errors, hence they represent all unknown effects, which should be isolated and removed from the travel times. The shot/station corrections are linearly dependent in equation (1); hence usually only their sum for a given ray (called “the total correction”) can be uniquely determined. The separation of shot/station corrections is possible, if at least one of shots is located near a station, so the corresponding corrections can be matched.

[15] The quantity of interest is the slowness S and its azimuthal variation. Assuming mostly horizontal propaga-

tion of refracted waves in a weakly anisotropic crust, we can put [Backus, 1965]

$$S = S_0(1 + A \cos 2\varphi + B \sin 2\varphi + C \cos 4\varphi + D \sin 4\varphi), \quad (2)$$

where $S_0 = 1/v_0$ is the slowness in the isotropic reference medium, v_0 is the velocity in the isotropic reference medium, φ defines the azimuth in which the wave propagates, and constants A , B , C , and D are small unknown coefficients which are linear combinations of the elastic parameters defining weak anisotropy. For weak transverse isotropy with a horizontal axis of symmetry, formula (2) simplifies to [Song *et al.*, 2001]

$$S = S_0(1 + E \cos 2(\varphi - \varphi_0) + F \cos 4(\varphi - \varphi_0)), \quad (3)$$

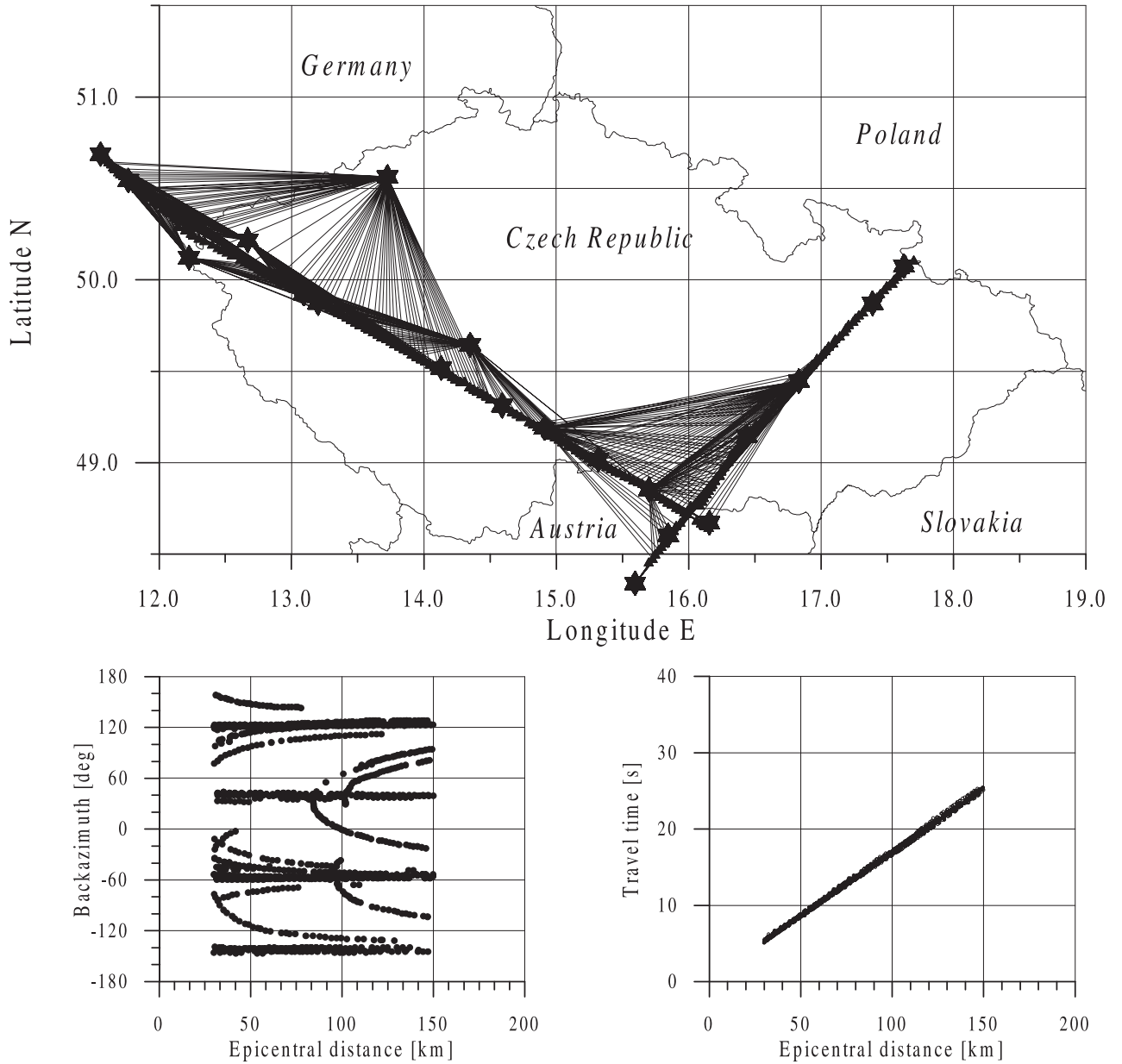


Figure 4. Ray path coverage for waves recorded by portable seismic stations. For details, see Figure 3 caption. The mean velocity calculated from the travel times is 6.013 km/s, and the offset at zero distance is 279 ms.

or, equivalently, to [Vavryčuk, 1997, equation 15]

$$S = S_0(1 + G \cos^2(\varphi - \varphi_0) + H \cos^4(\varphi - \varphi_0)), \quad (4)$$

where φ_0 is the angle defining the orientation of the symmetry axis in the horizontal plane, and E , F , G , and H are small unknown coefficients defining transverse isotropy. The azimuthal variation of velocity v can be expressed from equation (4) as

$$v = \frac{1}{S} = \frac{1}{S_0}(1 - G \cos^2(\varphi - \varphi_0) - H \cos^4(\varphi - \varphi_0)). \quad (5)$$

Equations (2)–(5) are valid only under weak anisotropy; hence they are applicable to anisotropy coefficients less than 0.1.

5. Inverse Problem

[16] The inversion is performed by minimizing two different misfit functions in the L2 norm: we minimize the absolute time residuals,

$$\chi_{\text{ABS}}^2 = \frac{1}{n-1} \sum (t_{ij} - \tau_{ij})^2 = \min, \quad (6)$$

and the relative time residuals,

$$\chi_{\text{REL}}^2 = \frac{1}{n-1} \sum \left(\frac{t_{ij} - \tau_{ij}}{t_{ij}} \right)^2 = \min, \quad (7)$$

where n is the total number of data, t_{ij} are the observed and τ_{ij} are the calculated travel times between the i th shot and

j th station. We use the two misfit functions in order to assess the reliability of the results obtained. Misfit function (6) represents a standard minimization procedure. Misfit function (7) reflects a varied quality of the observed data. The travel times measured at large epicentral distances are less accurate because the amplitudes of waves are more attenuated and less identifiable in noise. Hence higher travel times are automatically given lower weights proportional to $1/D_{ij}$.

[17] The minimization is performed with respect to the following sets of parameters: shot/station time corrections a_i and b_j , and parameters defining general weak anisotropy A , B , C , D , and S_0 (equation (2)) or alternatively parameters defining weak transverse isotropy G , H , S_0 , and φ_0 (equation (4)). The inverse problem is linear with respect to the shot/station corrections (40 parameters for the data set from permanent stations and 256 parameters for the data set from portable stations) and with respect to the parameters defining general anisotropy (5 parameters), but nonlinear with respect to the parameters defining transverse isotropy (4 parameters). Hence the inversion for general anisotropy is fully linear, but the inversion for transverse isotropy is partly nonlinear. The linear inversion for general anisotropy is performed using the singular value decomposition (SVD) matrix method [Press *et al.*, 1992, p. 51]. The inversion for transverse isotropy is split into two parts: linear (“internal”) and nonlinear (“external”). The nonlinear inversion is performed using Powell’s optimizing algorithm [Press *et al.*, 1992, p. 406]. The task of this optimization is to find the optimum values of anisotropy parameters G , H , S_0 , and φ_0 . The linear inversion uses the SVD matrix method and provides an optimum combination of shot/station corrections for each trial set of anisotropy parameters required for the nonlinear optimization.

6. Synthetic Tests

[18] In order to check the robustness of the inversion, we performed a series of synthetic tests for the ray geometries with permanent (see Figure 3) as well as portable (see Figure 4) stations. We preserved the number of stations and shots and their positions and assume a synthetic velocity model of the Earth crust formed by a homogeneous transversely isotropic half-space with the parameters

$$v_0 = 6.0 \text{ km/s}, G = H = -1.266 \times 10^{-2}, \varphi_0 = 60^\circ, \quad (8)$$

covered by a low-velocity isotropic layer. The propagation velocity in the half-space varies from 6.0 km/s in azimuth 150° to 6.152 km/s in azimuth 60° . The mean velocity is 6.066 km/s. The strength of anisotropy is 2.5%. The low-velocity layer is introduced by synthetic shot/station corrections, which are generated randomly with a uniform nonzero probability density in the interval from 0 to 1 s and with zero probability density elsewhere. Moreover, a synthetic Gaussian noise is superimposed on the theoretical travel times in order to simulate the properties of the observed data. The noise is generated with zero mean and with a standard deviation of 300 ms for permanent stations or 200 ms for portable stations, respectively. These values simulate errors present in the observed travel times caused mainly by inaccurate phase picking and by neglecting

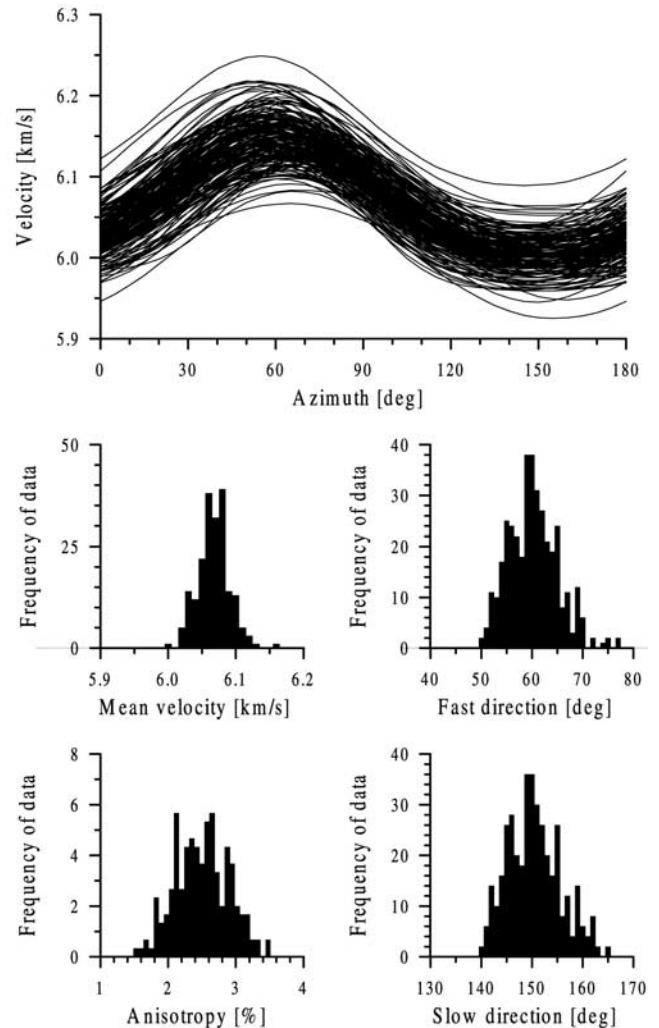


Figure 5. Results of the inversion of synthetic data for the permanent stations. (top) Azimuthal variation of velocity. (bottom) Histograms showing the scatter of the inverted parameters.

inhomogeneities in the crust. The synthetic travel times are inverted for values defined in equation (8). To obtain statistically relevant results, the noise superposition and the subsequent inversion were performed 200 times.

[19] Figures 5 and 6 present the results of the inversion for transverse isotropy (equation (4)) using misfit function (6) for the ray geometry with permanent and portable stations, respectively. The results are also summarized in Table 3. The upper plots in Figures 5 and 6 show the propagation velocity as a function of azimuth. Figures 5 and 6 show 200 inverted curves, each curve corresponding to a particular realization of the noise. It is evident that the family of curves in Figure 5 is much broader than that in Figure 6. This implies that the inversion of data from the portable stations yields remarkably more accurate results than that from the permanent stations. The error for portable stations is ~ 3 times lower than the error for permanent stations. This is caused mainly by the higher number of rays and by the higher accuracy of picking of arrival times achieved for the portable stations. Nevertheless, the curves surround the true velocity function

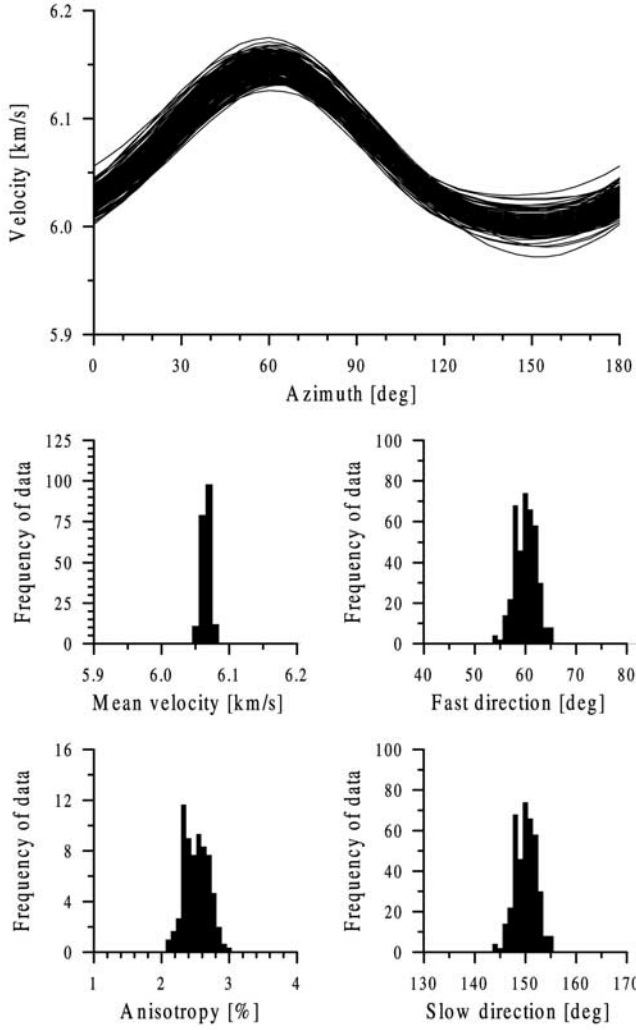


Figure 6. Same as in Figure 5 but for data from the portable stations.

in both cases, and the averaged curves approximate the exact curve quite accurately (see Table 3). The lower plots in Figures 5 and 6 show other statistical properties of the results: histograms of the mean velocity averaged over all azimuths, histograms of the azimuth of maximum and minimum velocities, and histograms of the strength of anisotropy. The mean velocity is calculated by

$$v_{\text{mean}} = \frac{1}{S_0} \left(1 - \frac{1}{2}G - \frac{3}{8}H \right), \quad (9)$$

obtained by averaging equation (5) and using the following identities:

$$\frac{1}{2\pi} \int_0^{2\pi} \cos^2 \varphi d\varphi = \frac{1}{2}, \quad \frac{1}{2\pi} \int_0^{2\pi} \cos^4 \varphi d\varphi = \frac{3}{8}. \quad (10)$$

The strength of anisotropy is defined as

$$\varepsilon = 2 \frac{v_{\text{max}} - v_{\text{min}}}{v_{\text{max}} + v_{\text{min}}} 100\%, \quad (11)$$

where v_{max} and v_{min} are the maximum and minimum propagation velocities, respectively. Figures 5 and 6 (bottom plots) show that all mentioned quantities approximate the exact values well. Hence the synthetic tests prove that the optimization procedure does not fall into false local minima of equation (6) or (7) corresponding to incorrect or significantly biased results, and that the inversion is well conditioned for both ray geometries. The tests also indicate that when inverting observed data, the azimuth of the maximum velocity should be found with an accuracy of several degrees, and anisotropy with strength of 2–3% should be reliably detected. Therefore we conclude that the ray path coverage, the extent and quality of the input data and the computing tools applied are sufficiently powerful to determine accurately the background isotropic velocity and the strength and orientation of the searched regional-scale anisotropy in the crust.

7. Results

[20] The observed data are inverted in a similar way as those in the synthetic tests. Instead of performing 200 independent perturbations around synthetic travel times, we now perform 200 independent perturbations around travel times calculated from the optimum velocity model found by the inversion. The procedure consists of the following steps: (1) Construction of an optimum velocity model corresponding to the observed travel times and determination of the shot/station corrections, (2) calculation of the theoretical travel times corresponding to the found optimum velocity model and shot/station corrections, (3) superposition of synthetic Gaussian noise with zero mean and with a standard deviation of 300 ms for permanent stations and of 200 ms for portable stations on the theoretical travel times, (4) inversion of the noisy theoretical travel times, and (5) 200 repetitions of steps 3 and 4 for different noise realizations.

Table 3. Inversion of Synthetic Data

Source of Data	Test Parameters				Test Results		
	Gaussian Noise Level, ms	Number of Stations	Number of Shots	Number of Data	Mean Velocity, km/s	Fast Direction, deg	Anisotropy, deg
<i>Optimization of Absolute Time Residuals</i>							
Portable stations	200	228	28	1475	6.066 ± 0.006	60 ± 2	2.51 ± 0.18
Permanent stations	300	19	21	135	6.068 ± 0.023	60 ± 5	2.47 ± 0.37
<i>Optimization of Relative Time Residuals</i>							
Portable stations	200	228	28	1475	6.065 ± 0.007	60 ± 3	2.47 ± 0.22
Permanent stations	300	19	21	135	6.071 ± 0.025	60 ± 7	2.35 ± 0.44
Exact values					6.066	60	2.5

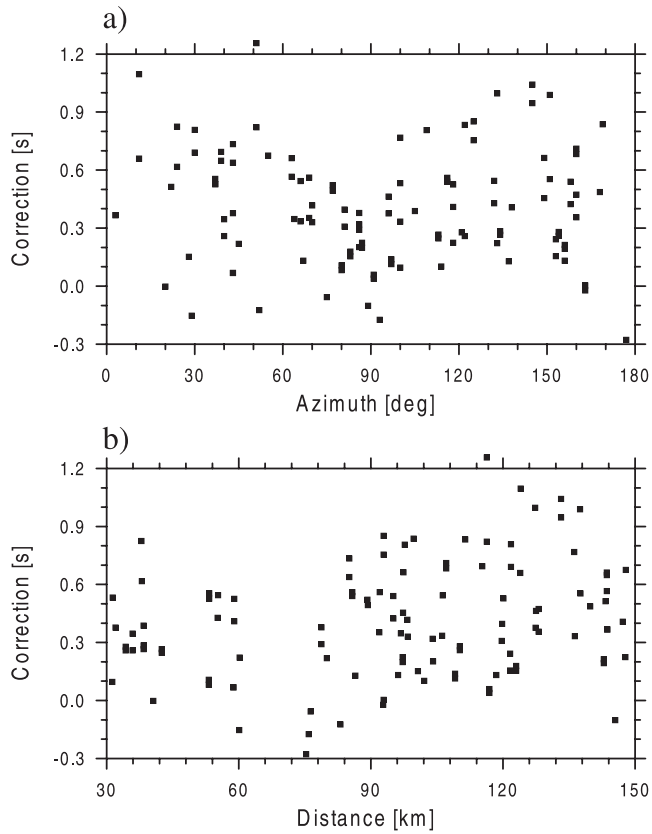


Figure 7. Total time corrections as a function of (a) azimuth and (b) epicentral distance.

[21] The results of the inversion are summarized in Table 4. Figures 7, 8, and 9 show the results if absolute time residuals (6) observed at permanent stations are minimized and a transversely isotropic medium (4) is assumed. Figures 10, 11, and 12 show the same for portable stations. The minimization reduced the standard deviation of time residuals from 422 ms to 271 ms for permanent stations and from 201 ms to 99 ms for portable stations. Nearly the same values are obtained if relative time residuals (7) are minimized (see Table 4).

7.1. Permanent Stations

[22] Figure 7 shows the total time corrections (the sum of the shot and station corrections for a given ray) as a function of azimuth and epicentral distance. We do not show shot/station corrections separately because of their linear dependency. The corrections vary from -0.3 s to 1.2 s and should reflect lateral inhomogeneities and systematic errors in picking of waves. The corrections display no significant trend indicating no or very weak dependence on the azimuth or epicentral distance. Figure 8 shows the retrieved azimuthal variation of the P_g velocity together with histograms quantifying its statistical properties. The figure indicates that the medium is anisotropic with the fast direction in $30\text{--}35^\circ$ and with strength of anisotropy of $2\text{--}3\%$. Figure 9 shows that the optimum velocity variation is almost independent of the inversion scheme used (linear or nonlinear). Figure 9 also shows that the observed data display a rather high scatter even though the shot/station

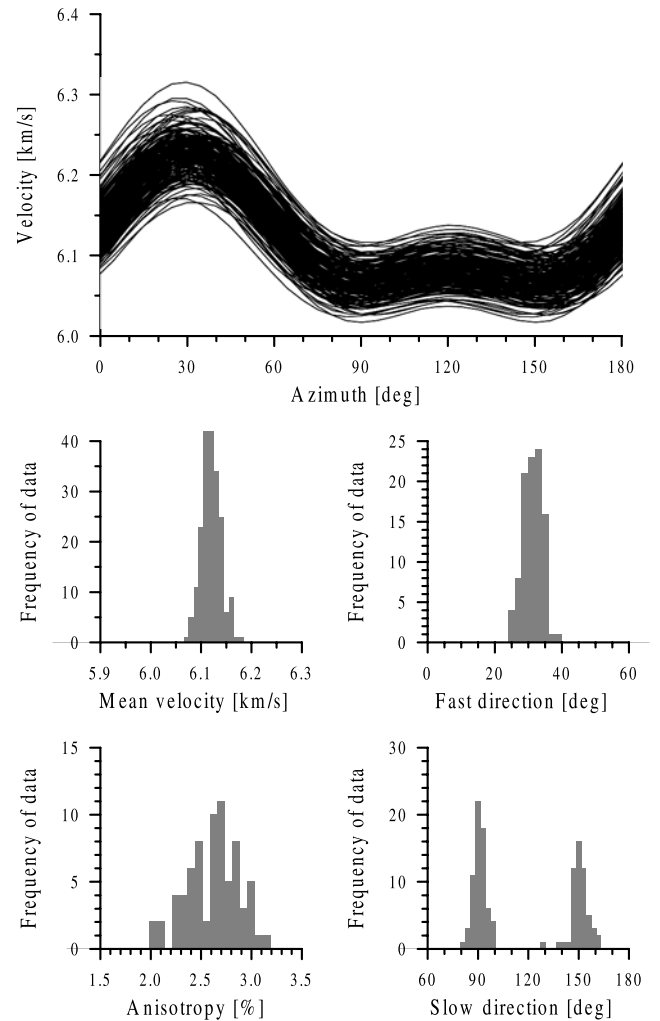


Figure 8. Results of the inversion from data observed at the permanent stations.

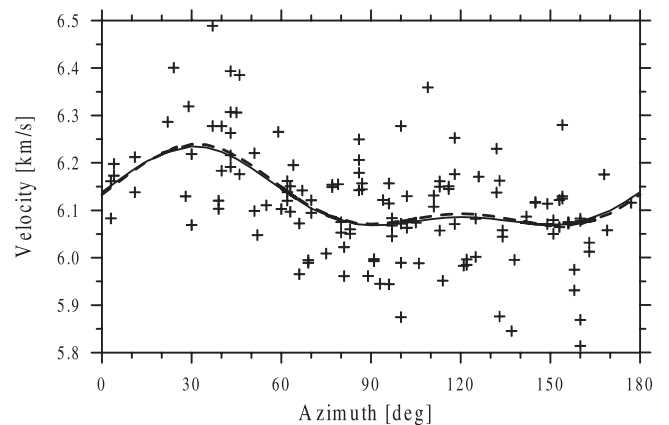


Figure 9. Optimum velocity variations under general weak anisotropy (dashed line) and weak transverse isotropy (solid line) calculated using equations (2) and (4) and data from permanent stations (marked by crosses).

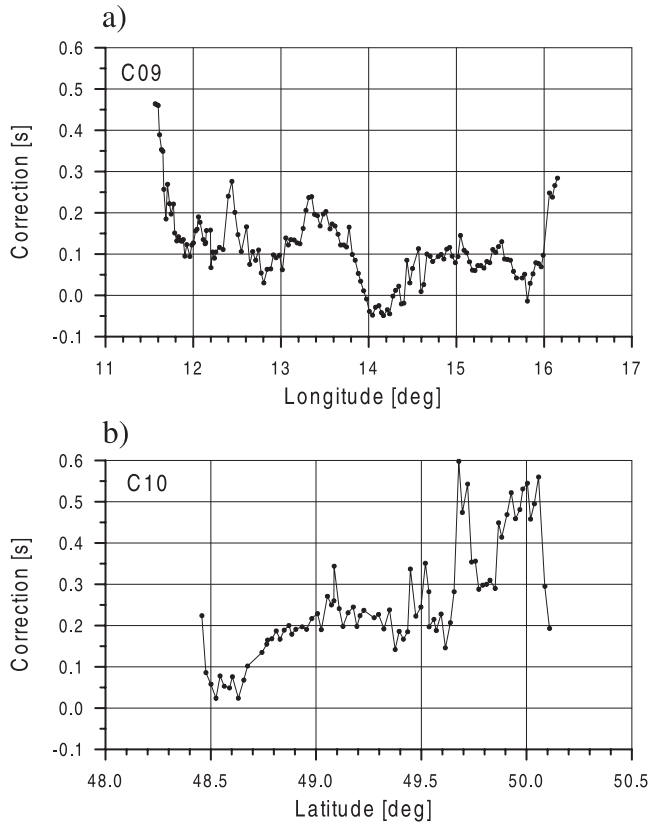


Figure 10. Station corrections along the (a) C09 and (b) C10 profiles.

corrections have been applied. This might indicate that effects owing to lateral inhomogeneities under a subsurface layer are at least of the same order as those owing to anisotropy.

7.2. Portable Stations

[23] Figure 10 shows the station corrections along the C09 and C10 profiles. We separated the station corrections from the total corrections owing to shots situated on the profiles. The corrections vary from -0.05 s to 0.6 s and display systematic trends, which correlate with a geological structure along both profiles.

[24] Looking at the C09 profile from NW (see Figure 10a), the high corrections (low velocities) at longitude 11.5°E are connected with Saxothuringian Carboniferous rocks. The mafic intrusions are manifested by low corrections (high velocities) around $11.8\text{--}12^\circ\text{E}$. The Saxothuringian crystalline complex (gneisses, migmatites) shows the corrections in $12\text{--}12.8^\circ\text{E}$. High values around 12.5°E coincide with Neogene sedimentary basins. Low values around 12.8°E are connected with mafic intrusions (amfibolite complex). The Barrandian unit (metasediments and Paleozoic strata) extends around $12.8\text{--}13.8^\circ\text{E}$. Low corrections in $13.8\text{--}14.3^\circ\text{E}$ can be associated with granitoid plutons with mafic intrusions (amfibolites, diabases, melaphyres) on the Barrandian/Moldanubian contact. The oscillations around 14.5°E can be connected with Tertiary and Quaternary sediments. The Moldanubian unit (gneisses, migmatites and granitoid intrusions) covers the interval $14.5\text{--}15.5^\circ\text{E}$. The Moravo-Silesian unit starts at 15.7°E

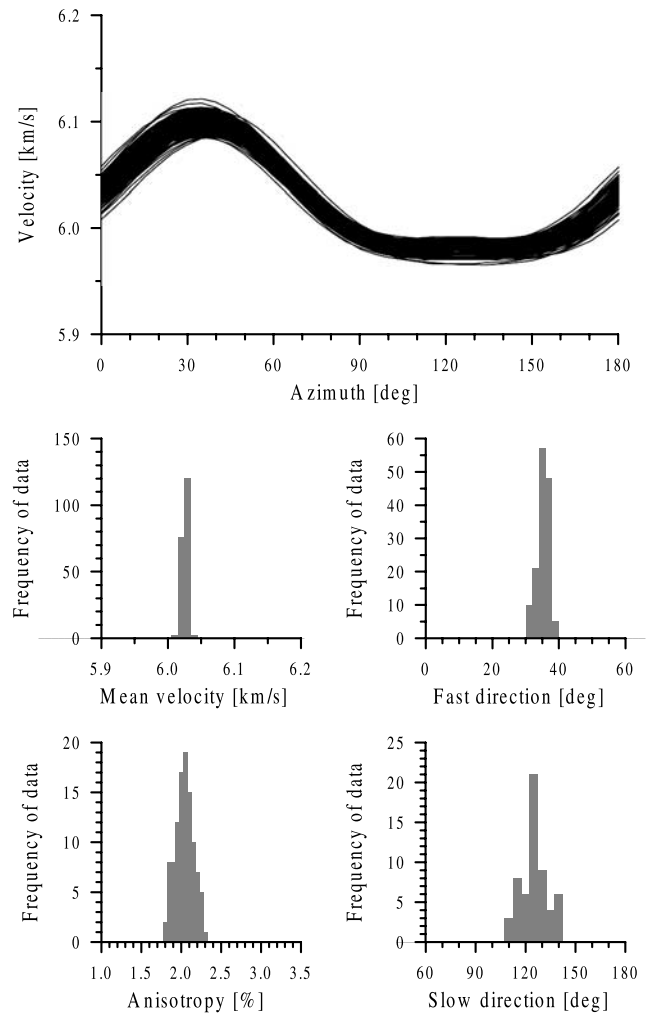


Figure 11. Results of the inversion from data observed at the portable stations.

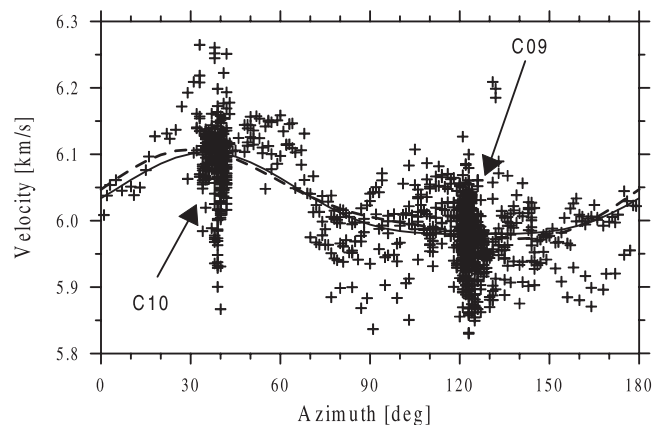


Figure 12. Optimum velocity variations under general weak anisotropy (dashed line) and weak transverse isotropy (solid line) calculated using equations (2) and (4) and data from portable stations (marked by crosses).

Table 4. Inversion of Observed Data

Source of Data	Inversion Parameters			Inversion Results				
	Number of Stations	Number of Shots	Number of Data	Mean Velocity, km/s	Fast Direction, deg	Slow Direction, deg	Anisotropy, %	Standard Deviation of Time Residuals, s
<i>Optimization of Absolute Time Residuals</i>								
Portable stations	228	28	1475	6.026 ± 0.004	35 ± 2	126 ± 9	2.04 ± 0.12	0.10
Permanent stations	19	21	135	6.121 ± 0.019	31 ± 3	121 ± 30	2.68 ± 0.25	0.27
<i>Optimization of Relative Time Residuals</i>								
Portable stations	228	28	1475	6.027 ± 0.005	39 ± 3	129 ± 6	1.46 ± 0.15	0.12
Permanent stations	19	21	135	6.041 ± 0.022	35 ± 5	125 ± 26	2.36 ± 0.41	0.31

and extends further to the SE to the Neogene sedimentary basin.

[25] The station corrections along the C10 profile (see Figure 10b) start with high values at latitude 48.4°N attributed to sediments. Then they show a low minimum in $48.5\text{--}48.7^\circ\text{N}$ corresponding to a crystalline metamorphic unit. Latitudes $48.7\text{--}49.4^\circ\text{N}$ define granitoid intrusions with Neogene sediments around 49.1°N . Paleozoic sediments of Carboniferous age coincide with oscillations in $49.4\text{--}49.7^\circ\text{N}$. The Neogene and Quaternary sediments produce high corrections in $49.7\text{--}49.8^\circ\text{N}$, while mafic intrusions lower the corrections around 49.8°N . High values in $49.8\text{--}50.1^\circ\text{N}$ correspond to Paleozoic Carboniferous rocks.

[26] The good correspondence between the station corrections and the geological structure under stations implies that the time term method used in the inversion is capable to effectively separate effects of subsurface inhomogeneities from those of anisotropy. Figure 11 shows the inversion results related to anisotropy. The retrieved anisotropy has the fast direction in 35° and strength of 2%. Figure 12 shows the optimum velocity variations for linear (2) and nonlinear (4) inversion schemes together with observed data after applying shot/station corrections. The figure indicates that the mean value of the P_g velocity along the C10 profile is distinctly higher than that for the C09 profile (despite a rather high scatter of the data along both profiles). The high-velocity anomaly is, however, observed not only for the C10 profile traversing the Moravo-Silesian unit but it is observed consistently for all rays in similar azimuths ($20\text{--}40^\circ$) crossing different geological units of the Bohemian Massif (see Figures 1 and 4). This implies that the anomaly can be attributed to anisotropy rather than to different crustal structures beneath the two profiles (e.g., high velocities in the Moravo-Silesian unit). The lateral inhomogeneities under a subsurface layer produce the scatter in the observed data (Figure 12).

7.3. Permanent and Portable Stations

[27] The results demonstrate that the data set from the portable stations (Figure 11) provides much higher accuracy than that from the permanent stations (Figure 8). The scatter of the curves displaying the azimuthal variation of velocity is much larger for the data from the permanent stations than for those from the portable stations. The same is evident from the corresponding histograms: the width of histograms is remarkably larger for the permanent than for the portable stations. The same effect has been observed in synthetic tests (Figures 5 and 6) and can be explained by the low number of travel times and low sampling frequency

for permanent stations. In spite of the different accuracy, the results of the inversion display a good stability and consistency with respect to the data set and the optimizing mode used. Either relative or absolute travel time residuals yield similar values for both data sets: the direction of the maximum velocity varies from 30° to 40° , the direction of the minimum velocity varies from 120° to 130° , and the anisotropy ranges from 1.5% to 2.5%. Also the azimuthal variations of velocity display similar shapes. Intriguingly, the azimuthal variations show well-defined maxima, but shallow and rather indistinct minima. The azimuthal variations retrieved from the permanent stations (Figures 8 and 9) even indicate the existence of two different minima with azimuths around 100° and 150° .

[28] Table 4 presents the retrieved values together with their errors calculated according to the procedure described above. We stress that the procedure is rather simple and able to provide only basic information on the stability of the inversion. The calculated errors, therefore, do not follow the errors of inverted values exactly. The actual errors should reflect many inconsistencies produced by simplifications in the numerical modeling (e.g., non-Gaussian distribution of noise in the observed data, inhomogeneities in deeper parts of the crust, varying orientation and strength of anisotropy, lower symmetry of anisotropy). As a consequence, the actual errors of the retrieved values may be larger than those estimated theoretically.

8. Discussion

[29] We found that the overall azimuthal velocity variation attributed to anisotropy is 1.5–2.5% and the direction of the maximum velocity is $\sim\text{N}35^\circ\text{E}$. Interestingly, similar anisotropy values have been detected also for the upper mantle anisotropy studied by P_n waves in the west of the Bohemian Massif (so far, no information on P_n anisotropy in the Bohemian Massif is available). Bamford [1977] studied the uppermost mantle P_n velocity beneath southern Germany from a dense network of refraction profiles and reported an anisotropy of 6–7% with the maximum velocity in the direction $\text{N}20^\circ\text{E}$. Enderle *et al.* [1996] updated this interpretation and reported an overall P wave anisotropy of 3–4% in a horizontal plane immediately below the Moho at a depth of 30 km with the maximum velocity in the direction $\text{N}31^\circ\text{E}$. The anisotropy increases to 11% at a depth of 40 km. Song *et al.* [2001] studied the uppermost mantle anisotropy in the western part of the Bohemian Massif and in Germany using regional earthquake P_n travel time data and obtained an anisotropy of 3.5–4% with the maximum velocity in the direction $\sim\text{N}25^\circ\text{E}$.

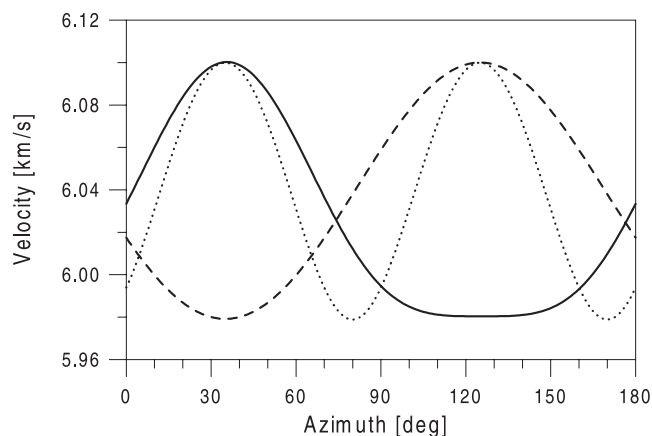


Figure 13. Velocity variations for the dry crack model (dashed line), fluid-filled crack model (dotted line), and for the observed anisotropy (solid line).

[30] The similar fast directions in the horizontal plane for the upper crustal and uppermost mantle anisotropy suggest a stable pattern of anisotropy orientation in the crust and the uppermost mantle in the Bohemian Massif and adjacent areas. However, the strength of the overall anisotropy seems to vary being lower in the crust than in the mantle. This is probably caused by heterogeneities, which are more pronounced in the crust, as well as by a high single-crystal anisotropy of olivine, the dominant component of the upper mantle. Obviously, the low value of crustal anisotropy on the regional scale does not exclude high values of anisotropy on the local scale. Measurements on rock samples frequently show anisotropy even higher than 10% [Pros *et al.*, 1998; Chlupáčová *et al.*, 2003], but a rather high scatter in orientations of the anisotropy axes and in the strength of anisotropy probably causes that the overall anisotropy in the crust is significantly suppressed.

[31] The orientation of the anisotropy axes can be compared with the present-day tectonic stress in the region. The stress measurements in the Bohemian Massif indicate a prevailing direction of the maximum compressive stress in the NW–SE direction with azimuths ranging from 125° to 150° [Peška, 1992]. A few exceptions exist in the southern part of the Bohemian Massif where the maximum compressive stress is indicated in the NE–SW direction. However, the NW–SE direction appears to be more reliable because it is more frequent and also consistent with the azimuth of $160^\circ \pm 10^\circ$ determined at the KTB drill hole [Brudy *et al.*, 1997] as well as with the azimuth of $144^\circ \pm 26^\circ$ determined for the overall stress orientation in western Europe [Müller *et al.*, 1992]. Hence the fast P_g velocity direction characterized by azimuth 35° is approximately perpendicular to the maximum horizontal compression in the region. A similar relation between anisotropy and tectonic stress has also been observed in other regions, for example in southern California [Hearn, 1996].

[32] The relation between anisotropy and present-day stress in the Bohemian Massif excludes the observed anisotropy to be primarily induced by the presence of either dry or fluid-filled stress-aligned cracks or microcracks [Kaneshima *et al.*, 1988; Crampin, 1994]. The dry crack model predicts the fast direction parallel to the maximum

compression, and the fluid-filled crack model predicts the fast directions parallel and perpendicular to the maximum compression [Crampin, 1984]. However, we observe only the fast direction perpendicular to the maximum compression. Hence the crack models predict azimuthal variations inconsistent with the observed variation (see Figure 13). Consequently, if the crack-induced anisotropy is present in the crust, then its effect should be minor. This could be an indication of a small differential stress in the region that prevents large populations of stress-aligned cracks from forming.

[33] Since the observed crustal anisotropy can hardly be explained by cracks aligned due to present-day stress, we suggest the anisotropy to originate in tectonically induced processes, probably during Variscan orogeny when the Bohemian Massif was sandwiched between opposing subduction zones of NE–SW trending. Such major tectonic activity could imprint the Bohemian Massif some preferentially oriented microstructural and macrostructural features like an alignment of rock-forming minerals (in the Moldanubian unit) or large-scale intrusion fabrics (in the Barrandian unit) responsible for the observed anisotropy at present. The coherent patterns of P_g and P_n anisotropy might indicate that anisotropy in the crust and uppermost mantle is of a similar origin.

[34] The crustal anisotropy determined from P_g waves can also be compared with the mantle anisotropy in the Bohemian Massif studied using the splitting of SKS waves. Assuming a homogeneous transverse isotropy with a horizontal symmetry axis in the crust and upper mantle, the polarization of the fast split S wave must be either parallel or perpendicular to the direction of the fast P wave velocity. Studies by Babuška and Plomerová [2000] and Plomerová *et al.* [2000] however show that the polarizations of split SKS waves do not match the directions of P_g or P_n anisotropy. This might be explained by the fact that P_g and P_n waves sample a shallow anisotropic structure, while the SKS results are more sensitive to lithospheric or upper mantle wide structures [Song *et al.*, 2001]. The discrepancy can also arise from an oversimplified anisotropy model, e.g., from the assumptions of a homogeneous transverse isotropy or the horizontal symmetry axis. For example, Babuška and Plomerová [2000] suggest dipping anisotropy structures in the lithosphere. The determination of anisotropy from prevalingly horizontally propagating P_g or P_n waves, which essentially is a 2-D method, cannot yield any such information.

9. Conclusions

[35] The consistency of the results obtained by applying different inversion schemes to different data sets indicates that the upper crust in the Bohemian Massif is anisotropic. The mean propagation velocity of P_g waves is 6.03 km/s. This value coincides well with 5.99 km/s obtained by Růžek *et al.* [2000] who studied the velocity model for the same area but from earthquake data. The high-velocity direction has an azimuth of $\sim N35^\circ E$, approximately perpendicular to the direction of the present-day maximum compression in the Bohemian Massif. The anisotropy is 1.5–2.5% with maximum and minimum velocities $v_{\max} = 6.10$ km/s and $v_{\min} = 5.98$ km/s, respectively. These values

characterize a regional-scale azimuthal anisotropy for ray paths of 30–190 km in length.

[36] The detected crustal anisotropy cannot be primarily caused by the presence of stress-aligned cracks or micro-cracks in the crust, which is the most common explanation for crustal anisotropy. The crack models predict the maximum velocity in the direction parallel to the maximum compression, but the opposite azimuthal velocity variation is observed. Hence, if the crack-induced anisotropy is present in the crust, then its effect should be minor.

[37] The high-velocity direction in the upper crust determined using *Pg* waves coincides well with that in the uppermost mantle studied using *Pn* waves (depth range 30–40 km). The anisotropy in the uppermost mantle is slightly higher (3–4%) and probably further increases with depth [Enderle et al., 1996]. The coherent patterns of *Pg* and *Pn* anisotropy can indicate that the anisotropy in the crust and uppermost mantle is of similar origin. We suggest that the detected crustal anisotropy is partly intrinsic and partly effective caused by a preferred orientation of rock-forming minerals and large-scale intrusion fabrics developed during the tectonic evolution of the Bohemian Massif.

[38] **Acknowledgments.** The authors thank Jaroslava Plomerová, Vladislav Babuška, Axel Plešinger, Ivan Pšenčík, and Cestmír Tomek for reading the manuscript and for their comments. The work was supported by the Grant Project 205/00/1350 of the Grant Agency of the Czech Republic and by the CELEBRATION 2000 Project financed by the Ministry of Environment of the Czech Republic. Seismic waveforms were obtained thanks to the CELEBRATION, WEBNET, and BOHEMA working groups, and the Czech, German and Polish seismological services. The assistance in data processing by Jan Švancara and Jana Pazzdírková from the Institute of Physics of the Earth in Brno, Czech Republic, is particularly appreciated.

References

- Babuška, V., and M. Cara, *Seismic Anisotropy in the Earth*, Kluwer Acad., Norwell, Mass., 1991.
- Babuška, V., and J. Plomerová, Saxothuringian-Moldanubian suture and predisposition of seismicity in the western Bohemian Massif, *Stud. Geophys. Geod.*, 44, 292–306, 2000.
- Backus, G. E., Possible forms of seismic anisotropy of the uppermost mantle under oceans, *J. Geophys. Res.*, 70, 3429–3439, 1965.
- Bamford, D., *Pn* velocity anisotropy in a continental upper mantle, *Geophys. J. R. Astron. Soc.*, 49, 29–48, 1977.
- Berckhemer, H., et al., Petrophysical properties of the 9-km-deep crustal section at KTB, *J. Geophys. Res.*, 102, 18,337–18,361, 1997.
- Brudy, M., M. D. Zoback, K. Fuchs, F. Rummel, and J. Baumgärtner, Estimation of the complete stress tensor to 8 km depth in the KTB scientific drill holes: Implications for crustal strength, *J. Geophys. Res.*, 102, 18,453–18,475, 1997.
- Chlupáčová, M., Z. Skácelová, and V. Nehybka, P-wave anisotropy of rocks from the seismic area in western Bohemia, *J. Geodyn.*, 35, 45–57, 2003.
- Crampin, S., Effective anisotropic elastic constants for wave propagation through cracked solids, *Geophys. J. R. Astron. Soc.*, 76, 135–145, 1984.
- Crampin, S., The fracture criticality of crustal rocks, *Geophys. J. Int.*, 118, 428–438, 1994.
- Dallmeyer, D., W. Franke, and K. Weber, *Pre-Permian Geology of Central and Eastern Europe*, Springer-Verlag, New York, 1994.
- Enderle, U., J. Mechie, S. Sobolev, and K. Fuchs, Seismic anisotropy within the uppermost mantle of southern Germany, *Geophys. J. Int.*, 125, 747–767, 1996.
- Franke, W., V. Haak, O. Oncken, and D. Tanner, (Eds.), *Orogenic Processes: Quantification and Modelling in the Variscan Belt*, *Geol. Soc. Spec. Publ.*, 179, 2000.
- Guterch, A., M. Grad, and G. R. Keller, Seismologists Celebrate The New Millennium with an Experiment in Central Europe, *Eos Trans. AGU*, 82(45), 529, 534, 536, 2001.
- Hearn, T. M., Anisotropic *Pn* tomography in the western United States, *J. Geophys. Res.*, 101, 8403–8414, 1996.
- Jahns, E., W. Rabbel, and S. Siegesmund, Quantified seismic anisotropy at different scales: A case study from the KTB crustal segment, *Z. Geol. Wiss.*, 24, 729–740, 1996.
- Kaneshima, S., M. Ando, and S. Kimura, Evidence from shear-wave splitting for the restriction of seismic anisotropy to the upper crust, *Nature*, 335, 627–629, 1988.
- Kern, H., and R. Schmidt, Physical properties of KTB core samples at simulated in situ conditions, *Scientific Drilling*, 1, 217–223, 1990.
- Kern, H., R. Schmidt, and T. Popp, The velocity and density structure of the 4000m crustal segment at the KTB drilling site and their relationship to lithological and microstructural characteristics of the rocks: An experimental approach, *Sci. Drill.*, 2, 130–145, 1991.
- Málek, J., M. Brož, T. Fischer, J. Horálek, P. Hrubcová, J. Janský, O. Novotný, and B. Růžek, Seismic measurements along short profiles in western Bohemia during the Celebration 000 experiment, *Acta Montana. A*, 18(12), 15–28, 2001.
- Martínková, M., Z. Pros, K. Klíma, T. Lokajčiček, and J. Kotková, Experimentally determined P-wave velocity anisotropy for rocks related to the western Bohemia seismoactive region, *Stud. Geophys. Geod.*, 44, 581–589, 2000.
- Matte, P., The Variscan collage and orogeny (480–290 Ma) and the tectonic definition of the Armorica microplate: A review, *Terra Nova*, 13, 122–128, 2001.
- Matte, P., H. Maluski, P. Rajlich, and W. Franke, Terrane boundaries in the Bohemian Massif: Result of large-scale Variscan shearing, *Tectonophysics*, 177, 151–170, 1990.
- Müller, B., M. L. Zoback, K. Fuchs, L. Mastin, S. Gregersen, N. Pavoni, O. Stephansson, and C. Ljunggren, Regional patterns of tectonic stress in Europe, *J. Geophys. Res.*, 97, 11,783–11,803, 1992.
- Peška, P., Stress indications in the Bohemian Massif: Reinterpretation of borehole televiewer data, *Stud. Geophys. Geod.*, 36, 307–323, 1992.
- Pitra, P., J. P. Burg, and M. Guiraud, Late Variscan strike-slip tectonics between the Tepla-Barrandian and Moldanubian Terranes (Czech Bohemian Massif): Petrostructural evidence, *J. Geol. Soc. London*, 156, 1003–1020, 1999.
- Plomerová, J., V. Babuška, and L. Ruprechtová, Travel times of seismic waves propagating to the Bohemian Massif from the south-west direction, *Stud. Geophys. Geod.*, 25, 356–365, 1981.
- Plomerová, J., V. Babuška, and L. Ruprechtová, Velocities of seismic waves propagating through the Bohemian Massif from foci in Poland, *Stud. Geophys. Geod.*, 28, 56–66, 1984.
- Plomerová, J., M. Granet, S. Judenherc, U. Achauer, V. Babuška, P. Jedlička, D. Kouba, and L. Vecsey, Temporary array data for studying seismic anisotropy of Variscan Massifs-the Armorican Massif, French Massif Central and Bohemian Masif, *Stud. Geophys. Geod.*, 44, 195–209, 2000.
- Press, W. H., S. A. Teukolsky, W. T. Vetterling, and B. P. Flannery, *Numerical Recipes in C: The Art of Scientific Computing*, Cambridge Univ. Press, New York, 1992.
- Pros, Z., T. Lokajčiček, R. Příkryl, A. Špičák, V. Vajdová, and K. Klíma, Elastic parameters of West Bohemian granites under hydrostatic pressure, *Pure Appl. Geophys.*, 151, 631–646, 1998.
- Rabbel, W., Seismic anisotropy at the Continental Deep Drilling Site (Germany), *Tectonophysics*, 232, 329–341, 1994.
- Rabbel, W., and W. D. Mooney, Seismic anisotropy of the crystalline crust: What does it tell us?, *Terra Nova*, 8, 16–21, 1996.
- Růžek, B., J. Zedník, K. Klíma, and L. Ruprechtová, Contribution of local seismic networks to the regional velocity model of the Bohemian Massif, *Stud. Geophys. Geod.*, 44, 175–187, 2000.
- Savage, M. K., Seismic anisotropy and mantle deformation: What have we learned from shear wave splitting?, *Rev. Geophys.*, 37, 65–106, 1999.
- Schulmann, K., J. Plomerová, V. Babuška, and O. Lexa, A kinematic model of the structural development of the Moldanubian root during the Variscan orogeny based on correlation of crustal and mantle lithosphere fabrics, *Geolines*, 14, 82–84, 2002.
- Song, L.-P., M. Koch, K. Koch, and J. Schlittenhardt, Isotropic and anisotropic *Pn* velocity inversion of regional earthquake traveltimes underneath Germany, *Geophys. J. Int.*, 146, 795–800, 2001.
- Vavryčuk, V., Crustal anisotropy from local observations of shear-wave splitting in West Bohemia, Czech Republic, *Bull. Seismol. Soc. Am.*, 83, 1420–1441, 1993.
- Vavryčuk, V., Reply to comments on “Crustal anisotropy from local observations of shear-wave splitting in West Bohemia, Czech Republic” by G. H. R. Bokelmann and J. Kawahara: Can the Hudson crack model describe behavior of real cracks?, *Bull. Seismol. Soc. Am.*, 85, 661–664, 1995.
- Vavryčuk, V., Elastodynamic and elastostatic Green tensors for homogeneous weak transversely isotropic media, *Geophys. J. Int.*, 130, 786–800, 1997.

- Weiss, T., S. Siegesmund, W. Rabbel, T. Bohlen, and M. Pohl, Seismic velocities and anisotropy of the lower continental crust: A review, *Pure Appl. Geophys.*, 156, 97–122, 1999.
-
- E. Brueckl, Vienna University of Technology, Gusshausstrasse 27-29, A-1040 Vienna, Austria. (ebrueckl@luna.tuwien.ac.at)
- Z. Hajnal, Department of Geological Sciences, University of Saskatchewan, 114 Science Place, Saskatoon, Saskatchewan, Canada S7N 5E2. (zoltan.hajnal@usask.ca)
- M. Grad, Institute of Geophysics, University of Warsaw, Pasteura 7, PL-02-093 Warsaw, Poland. (mgrad@mimuw.edu.pl)
- P. Hrubcová, B. Růžek, A. Špičák, V. Vavryčuk, and J. Zedník, Geophysical Institute, Academy of Sciences of the Czech Republic, Bcni II/1401, 141 31 Prague 4, Czech Republic. (pavla@ig.cas.cz; ruzek@ig.cas.cz; als@ig.cas.cz; vv@ig.cas.cz; jzd@ig.cas.cz)
- A. Guterch, Institute of Geophysics, Polish Academy of Sciences, Ks. Janusza 64, PL-04-152 Warsaw, Poland. (aguterch@igf.edu.pl)
- G. R. Keller, Department of Geological Sciences, University of Texas at El Paso, El Paso, TX 79968, USA. (keller@geo.utep.edu)
- K. Posgay, Eötvös Loránd Geophysical Institute, Kolumbusz u. 17-23, H-1145 Budapest, Hungary. (elgi@elgi.hu)
- O. Selvi, TUBITAK-MAM, Marmara Research Center, P.O. Box 21, 41470 Gebze/Kocaeli, Turkey. (selvi@yunus.mam.gov.tr)
- H. Thybo, Geological Institute, University of Copenhagen, Oster Voldgade 10, DK-1350 Copenhagen, Denmark. (thybo@geol.ku.dk)
- J. Vozár, Institute of Geology, Dubravská cesta 9, P.O. Box 106, 840 05 Bratislava 45, Slovakia. (geoljovo@savba.sk)